WATER RESEARCH ▮ (▮▮▮▮) ▮▮▮–▮▮▮

Available at www.sciencedirect.com

ScienceDirect

journal homepage: www.elsevier.com/locate/watres

The inhibitory effects of silver nanoparticles, silver ions, and silver chloride colloids on microbial growth

Okkyoung Choi[a], *Kathy Kanjun Deng*[b], *Nam-Jung Kim*[c], *Louis Ross Jr.*[d], *Rao Y. Surampalli*[e], *Zhiqiang Hu*[a,*]

[a]*Department of Civil and Environmental Engineering, University of Missouri, E2509 Lafferre Hall, Columbia, MO 65211, USA*
[b]*School of Engineering, Rice University, USA*
[c]*Department of Mechanical and Aerospace Engineering, University of Missouri, USA*
[d]*Electron Microscopy Core Facility, University of Missouri, USA*
[e]*Region 7 Office, US Environmental Protection Agency, Kansas City, KS, USA*

ARTICLE INFO

Article history:
Received 9 October 2007
Received in revised form
22 February 2008
Accepted 26 February 2008

Keywords:
Silver nanoparticles
Silver ion
AgCl colloid
Microbial growth
Nitrification
Inhibition

ABSTRACT

Emerging nanomaterials are of great concern to wastewater treatment utilities and the environment. The inhibitory effects of silver nanoparticles (Ag NPs) and other important Ag species on microbial growth were evaluated using extant respirometry and an automatic microtiter fluorescence assay. Using autotrophic nitrifying organisms from a well-controlled continuously operated bioreactor, Ag NPs (average size = 14±6 nm), Ag^+ ions ($AgNO_3$), and AgCl colloids (average size = 0.25 μm), all at 1 mg/L Ag, inhibited respiration by 86±3%, 42±7%, and 46±4%, respectively. Based on a prolonged microtiter assay, at about 0.5 mg/L Ag, the inhibitions on the growth of *Escherichia coli* PHL628-gfp by Ag NPs, Ag^+ ions, and AgCl colloids were 55±8%, 100%, and 66±6%, respectively. Cell membrane integrity was not compromised under the treatment of test Ag species by using a LIVE/DEAD Baclight™ bacterial viability assay. However, electron micrographs demonstrated that Ag NPs attached to the microbial cells, probably causing cell wall pitting. The results suggest that nitrifying bacteria are especially susceptible to inhibition by Ag NPs, and the accumulation of Ag NPs could have detrimental effects on the microorganisms in wastewater treatment.

1. Introduction

Nanosilver (silver nanoparticle, Ag NP) materials have a wide range of applications including spectrally selective coating for solar energy absorption (Rand et al., 2004; Cole and Halas, 2006), catalysis in chemical reactions (Zhai et al., 2006), surface-enhanced Raman scattering for imaging (Yamamoto and Watarai, 2006), and antimicrobial sterilization (Savage and Diallo, 2005; Sambhy et al., 2006; Pal et al., 2007). Because of their effective antimicrobial properties and low toxicity toward mammalian cells, Ag NPs have become one of the most commonly used nanomaterials in consumer products (104 out of 502 nanoproducts surveyed) (Maynard and Michelson, 2006). These nanoparticles will likely enter the sewage pipes and the wastewater treatment plants (WWTPs). At present, little is known about the adverse effects of Ag NPs on wastewater treatment and the environment.

It is known, however, that free silver ion (Ag^+) is highly toxic to a wide variety of organisms including bacteria. Metal toxicity to planktonic species such as algae (Lee et al., 2005) and bacteria (Hu et al., 2002, 2003) is often governed by the concentrations of aqueous free metal species (i.e., Ag^+). The inhibitory effect of Ag^+ is believed to be due to its sorption to the negatively charged bacterial cell wall, deactivating

*Corresponding author. Tel.: +1 573 884 0497; fax: +1 573 882 4784.
E-mail address: huzh@missouri.edu (Z. Hu).
0043-1354/$ - see front matter © 2008 Elsevier Ltd. All rights reserved.
doi:10.1016/j.watres.2008.02.021

Please cite this article as: Choi, O., et al., The inhibitory effects of silver nanoparticles, silver ions, and silver chloride colloids on microbial growth. Water Res. (2008), doi:10.1016/j.watres.2008.02.021

cellular enzymes, disrupting membrane permeability, and ultimately leading to cell lysis and death (Ratte, 1999; Sambhy et al., 2006). The aqueous concentrations of Ag^+ are typically low in wastewater treatment systems or in the natural environment because of its strong complexation with various ligands such as chloride ($K_{sp} = 10^{-9.75}$), sulfide ($K_{sp} = 10^{-49}$), thiosulfate, and dissolved organic carbon (Shafer et al., 1998; Wang, 2003). As a result, silver toxicity to microorganisms is generally not observed.

Nanosilver, a particle of Ag element, is a new class of material with remarkably different physiochemical characteristics such as increased optical, electromagnetic and catalytic properties from the bulk materials (Wenseleers et al., 2002; Kelly et al., 2003). Nanoparticles with at least one dimension of 100 nm or less have unique physicochemical properties, such as high catalytic capabilities and ability to generate reactive oxygen species (ROS) (Limbach et al., 2007) (see recent review by Nel et al., 2006). Silver in the form of nanoparticles could be therefore more reactive with its increased catalytic properties and become more toxic than the bulk counterpart. Furthermore, toxicity is presumed to be size- and shape-dependent (Pal et al., 2007), because small size nanoparticles (e.g., <10 nm) (Kloepfer et al., 2005; Morones et al., 2005) may pass through cell membranes and the accumulation of intracellular nanoparticles can lead to cell malfunction.

Little work has been done to evaluate the inhibition of microbial growth by different Ag species, especially Ag NPs in wastewater treatment systems where such information is valuable for operation planning and control. Both autotrophic and heterotrophic microorganisms are important in wastewater treatment. While heterotrophs are responsible for organic and nutrient removal, autotrophs are responsible for nitrification that is considered as the controlling step in biological nitrogen removal because of the slow growth rate of nitrifying organisms and their sensitivity to temperature, pH, dissolved oxygen (DO) concentration, and toxic chemicals (Blum and Speece, 1991; Hu et al., 2002). Consequently, the objective of this research was to evaluate the impact of important Ag species such as Ag NPs, Ag^+ ions, and AgCl colloids on heterotrophic and autotrophic growth.

In this research work, Ag NPs and AgCl colloids with larger sizes were synthesized and characterized by UV–vis spectroscopy and electron microscopy. The inhibitory effects on the autotrophic and heterotrophic growth were determined by a short-term extant respirometric assay and an automatic microtiter assay, respectively. Environmental scanning electron microscopy (ESEM) was applied as a complementary technique to examine the microbial/nanoparticle interactions. The mode of action of nanosilver toxicity was finally discussed based on the results of membrane integrity using a LIVE/DEAD Baclight™ bacterial viability kit.

2. Materials and methods

2.1. Silver materials

2.1.1. Silver nanoparticles

Ag NPs were synthesized by reducing silver nitrate with sodium borohydrate ($NaBH_4$) and adding polyvinyl alcohol (PVA) (Aldrich) as the capping agent to control the growth of nanocrystals and agglomeration of nanoparticles. To dissolve PVA, a solution containing 0.06% (wt) PVA was heated to 100 °C and cooled down to room temperature before use. Silver particles were prepared by rapidly injecting 0.5 mL of 10 mM $NaBH_4$ into 20 mL PVA solution containing 0.25 mM silver nitrate at room temperature. After 5 min of stirring, the reaction mixture was stored at 4 °C before use.

2.1.2. Silver ions

A silver nitrate standard solution (14 mM, Fisher Scientific) was used as a source of Ag^+ ions.

2.1.3. Silver chloride colloids

Aliquots of 100 mg/L AgCl colloids were prepared freshly by vigorously mixing (700 rpm) 1 mL of 14 mM silver nitrate standard solution and 1 mL of 28 mM sodium chloride with 18 mL of distilled water. Twice as much sodium chloride as silver nitrate was added to ensure complete complexation with no residual Ag^+ ions in the colloidal solution (confirmed by Ag^+ measurements with an ion-selective electrode).

2.2. Microbial cultures

2.2.1. Autotrophic bacteria

The mixed and enriched nitrifying bacteria were cultivated in a continuously stirred tank reactor (14 L) operated at solids retention time of 20 d and hydraulic retention time of 1 d using seed from a local nitrifying activated sludge plant in Missouri, USA. The reactor was fed with an inorganic medium containing ammonium (8.3 mM, NH_4NO_3) as the sole energy source and requisite macro- and micronutrients (Table 1). Low concentrations of anions such as chloride and sulfate were present in the reactor to minimize their complexation potential with Ag^+ ions. Sodium carbonate (0.5 M) was intermittently added to maintain the reactor pH at 7.5 ± 0.1 and fulfilled both carbon and alkalinity requirements. After a few months of operation, mixed liquor was periodically withdrawn from the nitrifying reactor for batch respirometric studies.

2.2.2. Heterotrophic bacteria

The test heterotrophic bacterium was *Escherichia coli* PHL628-gfp, a gift from Dr. Anthony Hay at Cornell University. This strain tagged with a green fluorescence protein (GFP) was a derivative of the *E. coli* K12 that forms biofilms as a consequence of the over-expression of curli (Junker et al., 2006). The test strain was grown overnight on a mechanical shaker (200 rpm) at room temperature in a nutrient-rich medium (BBL™ containing 5 g/L Gelysate™ peptone and 3 g/L beef extract, pH 6.9 ± 0.2).

2.3. Silver species characterization

Aliquots of the prepared Ag NP suspensions were periodically scanned from 250 to 700 nm to obtain absorption spectra using a UV–vis spectrophotometer (Cary 50, Varian, CA). Additional aliquots were used to determine the stability of the Ag NPs by measuring the concentrations of Ag^+ ions in the

Please cite this article as: Choi, O., et al., The inhibitory effects of silver nanoparticles, silver ions, and silver chloride colloids on microbial growth. Water Res. (2008), doi:10.1016/j.watres.2008.02.021

Table 1 – Composition of the growth nutrients in reactor influent

Compound	Concentrations in reactor influent		
	mg/L	Cations (mM)	Anions (mM)
$Mg(NO_3)_2$	61	$0.41Mg^{2+}$	$0.82NO_3^-$
$Ca(NO_3)_2$	41	$0.25Ca^{2+}$	$0.25NO_3^-$
$NaNO_3$	879	$10.34Na^+$	$10.34NO_3^-$
NH_4NO_3	667	$8.33NH_4^+$ [a]	$8.33NO_3^-$
K_2HPO_4	3.9	$0.04K^+$	$0.02HPO_4^-$
$FeCl_2 \cdot 4H_2O$	2	$0.01Fe^{2+}$	$0.02Cl^-$ [b]
$MnSO_4 \cdot H_2O$	3.4	$0.02\ n^{2+}$	$0.02SO_4^{2-}$ [c]
$(NH_4)_6Mo_7O_{24} \cdot 4H_2O$ $0.001Mo_7O_{24}^{6-}$	1.2	$0.006NH_4^+$ [a]	
$CuSO_4$	0.8	$0.01Cu^{2+}$	$0.01SO_4^{2-}$ [c]
$Zn(NO_3)_2 \cdot 6H_2O$	1.8	$0.01Zn^{2+}$	$0.02NO_3^-$
$Ni(NO_3)_2 \cdot 6H_2O$	0.3	$0.001Ni^{2+}$	$0.002NO_3^-$

[a] Total $NH_4^+ = 8.336$ mM.
[b] Total $Cl^- = 0.02$ mM.
[c] Total $SO_4^{2-} = 0.03$ mM.

Ag NP suspensions using a silver ion/sulfide selective electrode (Denver instrument, Denver, CO).

The sizes of Ag NPs and AgCl colloids were characterized by an FEI Quanta 600F ESEM (resolution: 3 nm at 30 kV, FEI Company, OR) equipped with a scanning transmission electron microscopy (STEM) detector. The Ag NP suspension was added to standard carbon-coated TEM grid. Images of the samples were taken at an accelerating voltage of 30 keV.

2.4. *Autotrophic growth determined by extant respirometry*

Autotrophic growth inferred from oxygen uptake rates due to ammonia oxidation was measured in triplicate using a batch extant respirometric assay (Hu et al., 2002). Aliquots (60 mL) of nitrifying bacteria were collected from the nitrifying reactor. MOPS[3-(N-morpholino) propanesulfonic acid, pH adjusted to 7.5] at a final concentration of 20 mM was added to maintain relatively constant pH of 7.5 during ammonium oxidation. The nitrifying bacterial suspensions were amended with Ag NPs, Ag^+ ions and AgCl colloids individually at the final concentration range of 0.1–1 mg/L Ag, filled into the respirometric bottles with no headspace, and then tightly capped. Every batch respirometric test was accompanied by a positive control (e.g., untreated nitrifying bacteria only) at room temperature ($25 \pm 2\ ^\circ C$). The nitrifying bacterial suspensions were aerated with pure oxygen gas before aliquots of NH_4^+-N (10 mg/L N as NH_4NO_3) were injected. Magnetic stirring at ca. 100 rpm was provided in the bottles to ensure complete mixing. A decrease in the DO level in the respirometric vessel was measured by a DO probe (YSI model 5300A, Yellow Springs, OH) and continuously monitored at 4 Hz by an interfaced personal computer. The degree of inhibition of autotrophic microbial growth was inferred from the difference between the measured specific oxygen uptake rate in the absence and presence of the Ag species (Hu et al., 2002).

2.5. *Heterotrophic growth determined by an automated microtiter assay*

To evaluate the inhibitory effects of Ag species on heterotrophic growth, *E. coli PHL628-gfp* was grown in nutrient broth (BBL) at room temperature overnight. For the microtiter fluorescence assay, aliquots of the fresh medium (190 μL) were pipetted into eight parallel wells of a 96-well microplate (i.e., 8 replicates), and aliquots (10 μL) of overnight *E. coli cells* were inoculated in each well. Aliquots of the Ag NP suspension, Ag^+ or AgCl colloidal solution were added individually to each well to reach predetermined Ag concentrations. The cells were exposed to ambient air and mixed intermittently to support their growth on the plate. A program was made to incubate the samples with vigorous mixing for 10 s per hour before the fluorescence intensities (535 nm) excited at 485 nm were recorded automatically every hour for 24 h. The plate was pre-equilibrated at room temperature ($25 \pm 2\ ^\circ C$) for 0.5 h and the fluorescence (in relative fluorescence unit, RFU) of microbial suspensions was measured with a fluorescence microreader (VICTOR^3, PerkinElmer, Shelton, USA).

The time-dependent microbial growth associated with organic substrate oxidation in the 96-microwells was simulated using an exponential growth model:

$$X = X_0 e^{\mu t} \quad (1)$$

where X and X_0 are final and initial biomass concentrations, respectively, as reflected by the fluorescence intensity. The parameters of the specific microbial growth rate, μ, were determined via least-squares error analysis using the SOLVER routine in Microsoft Excel.

2.6. *Microbial/nanoparticle interaction*

The microbial/nanoparticle interaction was visualized using the FEI Quanta 600F SEM in the environmental (ESEM) mode that allows organic samples to be examined without applying a conductive coating prior to imaging. The enriched nitrifying culture amended with commercially available Ag NPs (10 nm, Nanostructured & Amorphous Materials, Inc., Houston, TX) was placed in an Al cup on a cold stage (10 °C) and imaged at ca. 7 Torr and 80% relative humidity. In order to obtain higher-resolution images, bacteria amended with our own Ag NPs were examined under high-vacuum conditions utilizing a back-scattered electron (BSE) detector. The nanoparticle samples synthesized in our laboratory were prepared using a standard protocol described above, critically point dried, and coated with ~10 nm of Pt.

2.7. *LIVE/DEAD bacterial viability assays*

Experiments were carried out in the presence and absence of nanoparticles to determine the cell viability of heterotrophic (*E. coli* PHL628 without GFP tagged) and autotrophic cultures by using a LIVE/DEAD Baclight^{TM} bacterial viability kit (Molecular Probes, Eugene, OR) (Hu et al., 2003). Viable and dead cells were detected by differential staining with a mixture of a green fluorochrome, SYTO 9 (stains all cells, live or dead), and a red fluorochrome, propidium iodide (stains

Please cite this article as: Choi, O., et al., The inhibitory effects of silver nanoparticles, silver ions, and silver chloride colloids on microbial growth. Water Res. (2008), doi:10.1016/j.watres.2008.02.021

only bacteria with damaged membranes). A reduction in the SYTO 9 fluorescent emission results when both dyes are present in the cell. Dead cells subject to 75% ethanol killing for 1 h were provided as a positive control. To reduce background fluorescence, the microbial suspension was washed with 0.85% $NaNO_3$ after centrifuging at 10,000*g* for 15 min. After adding aliquots of microbial suspensions and stain solution to each well of a 96-well microplate, the plate was incubated at room temperature in the dark for 15 min, and the relative fluorescence intensity was measured by the VICTOR fluorescence microreader. Enumeration of stained cells was facilitated by excitation at 485 nm and detection at 642 nm (red) and 535 nm (green), for propidium iodide and SYTO 9, respectively.

3. Results and discussion

3.1. *Characterization of Ag NPs and AgCl colloids*

The absorption spectrum (Fig. 1) of dark brown Ag NPs prepared by chemical reduction showed a surface plasmon absorption band with a maximum of about 400 nm, a characteristic peak of Ag NPs (Petit et al., 1993; Kong and Jang, 2006), indicating the presence of Ag NPs in the solution. Due to the excitation of plasma resonances or interband transitions, some metallic nanoparticle dispersions exhibit unique bands/peaks (Creighton and Eadont, 1991). The broadness of the peak is a good indicator of the size of nanoparticles. As the particle size increases, the peak becomes narrower with a decreased bandwidth and an increased band intensity (Petit et al., 1993; Kong and Jang, 2006). Furthermore, there is an inverse linear relationship between the full-width at half-maximum (FWHM) and the diameter of particles (Petit et al., 1993):

$$\mathrm{FWHM} = 50 + \frac{230}{D} \quad (2)$$

where both FWHM and the particle diameter (D) are in nanometers. The size of the Ag NPs was estimated as approximately 16 nm based on Eq. (2). This result is consistent with the STEM results, which showed a size distribution between 10 and 40 nm (Fig. 2) of the Ag NPs with an average of 14 ± 6 nm.

A shoulder at approximately 425 nm was noticed in UV–vis absorption spectra, indicating a broad distribution of particle sizes and shapes in the solution because of crystallization, as was confirmed by STEM imaging. The position and the number of peaks in the absorption spectra are dependent on the shape of the particles: for an ellipsoidal particle there are two peaks whereas for spherical silver particles there is only one peak centered at about 400 nm (Creighton and Eadont, 1991; Petit et al., 1993).

The concentrations of Ag^+ ions were measured simultaneously to evaluate the stability of Ag NPs in the suspension. The beginning Ag^+ concentration to make the Ag NP suspensions was 27 mg/L (0.25 mM). At the completion of the reaction, the residual Ag^+ concentration was 0.6 ± 0.1 mg/L. The Ag^+ concentration remained largely unchanged at the end of 1 day of resting at room temperature. Afterward, the Ag^+ concentrations increased gradually (data not shown), as also indicated from the changes of solution color.

During a week of Ag^+ monitoring at room temperature, the color of Ag NP suspensions changed from dark brown to

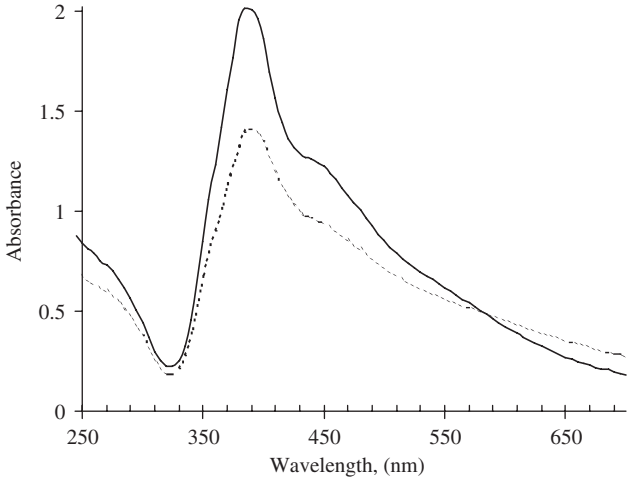

Fig. 1 – UV–vis absorption spectra of an Ag NP suspension recorded immediately after chemical reduction (solid line) and after 1 week (dash line) at room temperature.

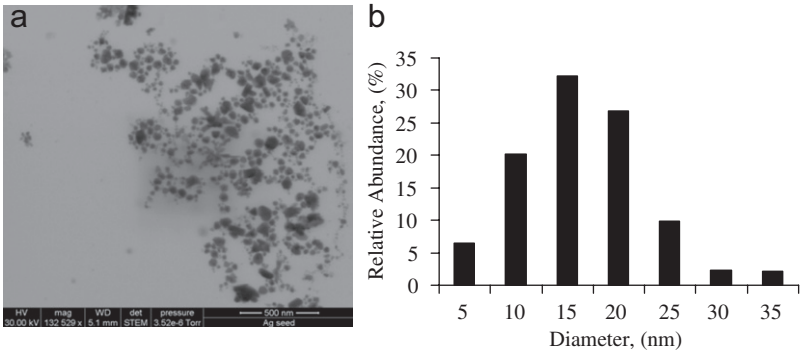

Fig. 2 – STEM image of Ag NPs prepared by chemical reduction (a) and the particle size distribution (b). The average particle size was 14 nm. Bar size: 500 nm.

Please cite this article as: Choi, O., et al., The inhibitory effects of silver nanoparticles, silver ions, and silver chloride colloids on microbial growth. Water Res. (2008), doi:10.1016/j.watres.2008.02.021

yellow, presumably due to oxidative dissolution of the Ag NPs

$$4Ag + O_2 + 2H_2O = 4Ag^+ + 4OH^- \quad (3)$$

The color change associated with particle dissolution and the presence of multiple UV–vis absorption bands indicate the existence of Ag NPs of various shapes and sizes, as was confirmed by STEM imaging (Fig. 2). To minimize the interference of dynamic changes of Ag NPs, we used the freshly prepared Ag NP suspensions that were stored shortly (a few days) at 4 °C before use, during which no significant changes of Ag^+ concentrations were observed in the suspension (data not shown).

Silver chloride colloids (100 mg/L Ag) were prepared with an average size of ca. 0.25 μm. The particle sizes ranged from 0.1 to 2 μm. A constant low Ag^+ concentration was detected because of the overdose of chloride. The fraction of Ag^+ was measured to be less than 0.1% of the total Ag in the AgCl colloidal solution.

3.2. *Effect of Ag species on autotrophic growth*

An extant respirometric technique was developed to determine biokinetic parameters from small pulses of substrate (e.g., NH_4^+) while minimizing changes in the microbial physiological state (Chandran and Smets, 2000; Hu et al., 2002). Fig. 3 shows a representative respirograph of ammonia oxidation after an aliquot of ammonium was injected at ~100 s in the enriched nitrifying microbial suspension. The lack of change in DO illustrates nitrification inhibition in the presence of Ag NPs. There was no significant pH change before and after the test because of the addition of MOPS.

As shown in Fig. 4, at 1 mg/L Ag in the nitrifying suspension, the inhibitions by Ag NPs, Ag^+ ions, and AgCl colloids were 86 ± 3%, 42 ± 7%, and 46 ± 4%, respectively. Of all the Ag species tested, Ag NPs presented the highest inhibition on nitrifying bacterial growth. Interestingly, the freshly prepared AgCl colloids with an average size of 0.25 μm also inhibited nitrification. At the same level of Ag dose, there was no statistical difference ($p > 0.05$) of inhibition between AgCl colloids and Ag^+ ions. At this small size, silver chloride colloids appeared to reduce the bacterial growth as effectively as Ag^+.

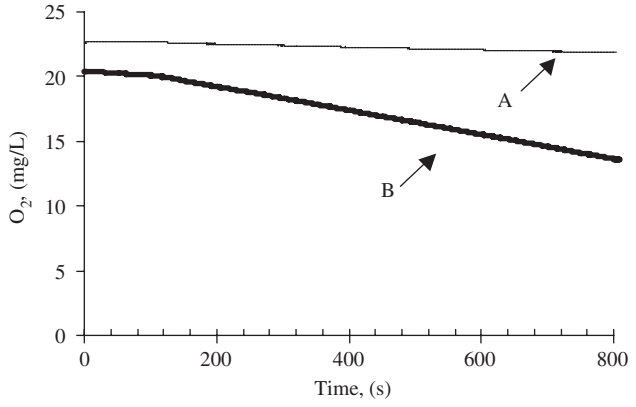

Fig. 3 – Nitrification inhibition inferred from the decrease of specific oxygen uptake rate (slope of curve A) in the presence of Ag NPs, as compared with control (curve B) after an aliquot of ammonium nitrate was injected individually at approximately 100 s.

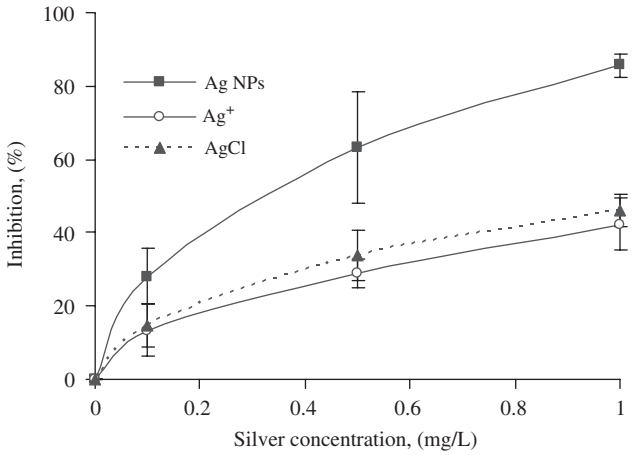

Fig. 4 – Nitrification inhibition as a function of the concentrations of silver in the form of Ag NPs, Ag^+ ions, and AgCl colloids. Error bars indicate one standard deviation.

3.3. *Effect of Ag species on heterotrophic growth*

Consistent with the results from autotrophic growth study, Ag NPs inhibited *E. Coli* growth. While no inhibition was observed at Ag NP concentrations below 1.0 μM, the heterotrophic growth rate was reduced significantly by 55% as the Ag NP concentrations increased to 4.2 μM (Table 2). The IC 50 inhibition by the Ag NP suspension, or the half maximal inhibitory concentration, was estimated to be 4.0 μM ($n = 8$). Surprisingly, silver ion was the most toxic species to inhibit heterotrophic growth. At 4.2 μM (~0.5 mg/L Ag), the inhibitions on the growth of *E. coli* PHL628-gfp were 55 ± 8%, 100%, and 66 ± 6% by Ag NPs, Ag^+ ions, and AgCl colloids, respectively. *E. Coli* treated with 1 mg/L Ag (or 9.3 μM) in the forms of Ag NPs, Ag^+ ions, or AgCl did not exhibit signs of growth (data not shown). The inhibition on heterotrophic growth appeared to be more severe from the long-term microtiter fluorescence assays, as we reported earlier that inhibition on microbial growth with longer period of metal exposure tends to be more significant (Hu et al., 2004).

A slight lag phase of *E. coli* growth (~1.5 h) was observed during the automatic microtiter assays (Fig. 5). Stationary phase was reached after incubation of the heterotrophic strain for approximately 12 h at room temperature (25 ± 1 °C). Upon the addition of Ag NPs in the microbial suspension, a slight decrease of fluorescence efficiency (i.e., fluorescence quenching) with increasing Ag NP concentrations was observed. In the case of AgCl colloids, the quenching effect was less significant (data not shown). The results are consistent with the existing experimental data (Sabatini et al., 2007; Yamaguchi et al., 2007), indicating that the overlap between the GFP-tagged microbial fluorescence and the plasmon absorption of Ag nanoparticles may slightly

Please cite this article as: Choi, O., et al., The inhibitory effects of silver nanoparticles, silver ions, and silver chloride colloids on microbial growth. Water Res. (2008), doi:10.1016/j.watres.2008.02.021

Table 2 – Specific growth rates (μ) of *E. coli PHL628-gfp* and the inhibitions by silver species at different concentrations

Concentration (μM)	Ag NP		Ag^+		AgCl colloid	
	μ (d^{-1})	Inhibition (%)	μ (d^{-1})	Inhibition (%)	μ (d^{-1})	Inhibition (%)
1.4	0.40 (±0.03)	17 (±5)	0.41 (±0.02)	11 (±4)	0.43 (±0.01)	7 (±4)
2.8	0.34 (±0.03)	30 (±6)	0.14 (±0.03)	69 (±6)	0.35 (±0.02)	24 (±5)
4.2	0.22 (±0.04)	55 (±8)	0	100	0.16 (±0.03)	66 (±6)

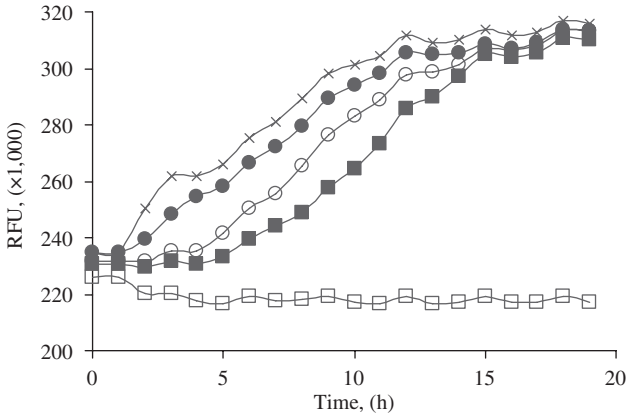

Fig. 5 – Effect of Ag NP concentrations (×, 0 μM; ●, 1.4 μM; ○, 2.8 μM; ■, 4.2 μM; □, 9.3 μM) on the growth of *E. coli* PHL628-gfp, as measured by relative fluorescence units.

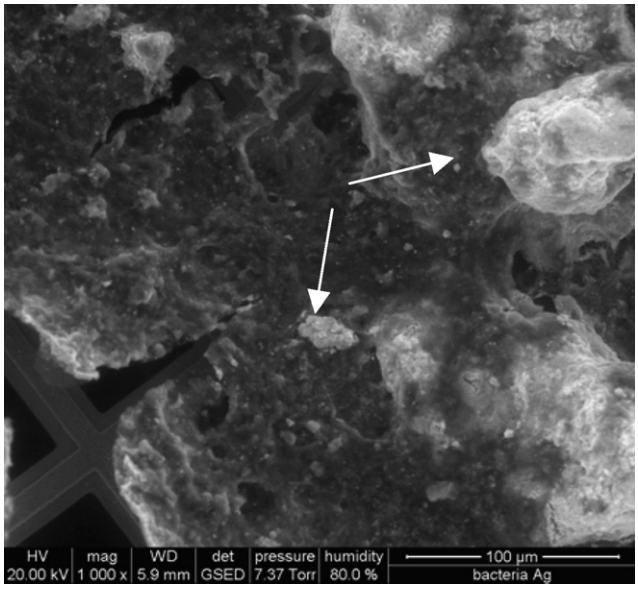

Fig. 6 – Silver nanoparticles adsorbed to the enriched nitrifying culture on a copper grid using ESEM. Arrows show aggregated AgNPs that attached to microbial cells or embedded in microbial extracellular polymeric substances. Bar size: 100 μm.

cause the quenching of the excited-state of GFP molecules on the Ag NPs.

3.4. *Microscopic observation of microbial/nanoparticle interaction*

The microbial–nanoparticle interaction was visualized by ESEM, a specialized technique capable of imaging hydrous samples without the need of pretreatment for conductive coating (Redwood et al., 2005; Priester et al., 2007). Commercially available Ag NPs (Nanostructured & Amorphous Materials, Inc., advertised powder size of 10 nm) aggregated in water and the nitrifying bacterial suspension. It appeared that the particles were embedded in microbial extracellular polymeric substances (Fig. 6). The true size (from 200 nm to a few μm) of Ag NPs in water suspension was significantly different from the claimed size of commercial nanopowders, consistent with the results reported by others (Adams et al., 2006).

Higher-resolution electron micrographs were obtained using BSE mode. After mixing a freshly prepared Ag NP suspension with the mixed and enriched nitrifying cultures, it appeared that Ag NPs were adsorbed to the microbial surfaces, probably causing cell wall pitting (Fig. 7). Additional work is underway to take higher-resolution images in order to better understand the microbial–nanoparticle interactions.

3.5. *Cell membrane integrity inferred from LIVE/DEAD assays*

The fluorescence intensities of the stained microbial cells at 535 nm (green) and 642 nm (red) represent live and dead cells, respectively. The green/red fluorescence ratio, obtained by dividing the green and red intensities, was applied to compare the difference among various treatments by Ag species. At 1 mg/L Ag, the ratio obtained from the microbial suspensions treated with Ag NPs showed no significant difference compared to controls ($P > 0.05$), indicating that there is no evidence of cell membrane leakage caused by Ag NPs. Similar results were observed in samples treated with Ag^+ ions or AgCl colloids.

3.6. *Inhibition comparison and mode of antimicrobial action*

Among the Ag species tested, the freshly prepared Ag NPs presented the highest inhibition to autotrophic nitrifying organisms. In contrast, silver ion appeared to be most toxic to heterotrophic growth. Different experimental assays chosen

Please cite this article as: Choi, O., et al., The inhibitory effects of silver nanoparticles, silver ions, and silver chloride colloids on microbial growth. Water Res. (2008), doi:10.1016/j.watres.2008.02.021

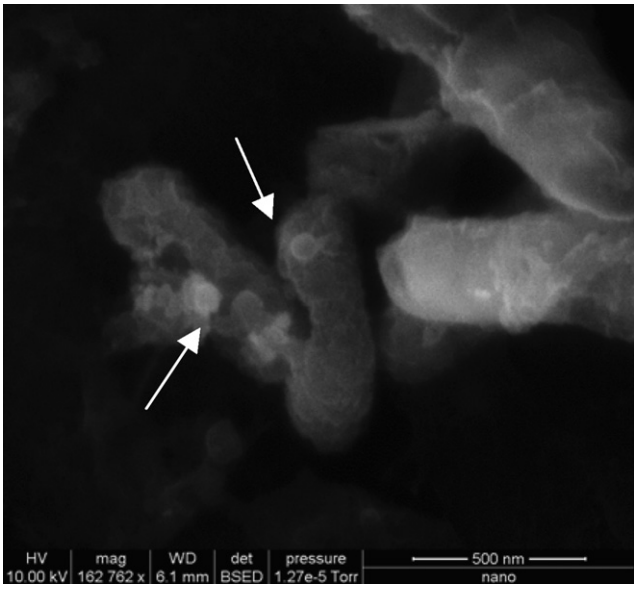

Fig. 7 – Silver nanoparticles adsorbed to the enriched nitrifying culture using a high-speed BSE detector. Arrows show spherical or hexagon types of Ag NPs that attached to the microbial cells, probably causing cell wall pitting. Bar size: 500 nm.

for the enriched nitrifying bacteria and heterotrophic *E. coli* cells made it difficult to compare the toxicity of Ag NPs to the two different bacterial species. The difference in toxicity may be attributed to different growth conditions and cell properties. The nitrifying bacteria were completely mixed in the respirometric bottles, aerated with pure oxygen and their activities were monitored by oxygen uptake rate measurements. Conversely, the *E. coli* cells were mixed intermittently in microwells, aerated with ambient air and their activities were inferred from fluorescence measured over a prolonged period of time (~1 d). Because they have a faster growth rate than nitrifying bacteria, *E. coli* cells may have stronger oxidizing/reducing power and interact with Ag species to form cell-particle aggregates (Sondi and Salopek-Sondi, 2004; Kahraman et al., 2007), as visible from Figs. 6 and 7, or produce extracellular or intracellular Ag NPs (Efrima and Bronk, 1998), causing more complex growth problems. Nitrifying bacteria have remarkably complex internal membrane systems where ammonia monooxygenase (AMO, responsible for ammonia oxidation to produce hydroxylamine, NH_2OH) is located, whereas hydroxylamine oxidoreductase (HMO) is located in the periplasm (Madigan et al., 2000). Therefore, we speculate that Ag NPs may have a direct impact on nitrifying cell membranes where key ammonia oxidation enzymes are located.

The use of PVA during the synthesis of Ag NPs to control the nanoparticles size could affect the antibacterial activity by the coverage of PVA on AgNPs to prevent the direct contact with bacteria. Due to the significant dilution (1:25 or higher) of the Ag NP suspension and solvent competition in cell cultures, the effect of PVA on nanosilver toxicity, however, would be minimal.

Nanoparticles have substantially different physiochemical properties from those of bulk materials of the same composition, possibly resulting in different toxicity mechanisms to biological systems (Nel et al., 2006). The mode of antimicrobial action by Ag NPs could be the inhibition of the microbial processes on the cell surface and in the cell. Previous research demonstrated that Ag NPs attach to the surface of cell membrane, causing the change of membrane permeability, dissipation of the ATP pool and proton motive force, and finally cell death (Sondi and Salopek-Sondi, 2004; Morones et al., 2005; Lok et al., 2006). The results from our bacterial viability tests indicated that there is no evidence of the cell membrane leakage caused by any Ag species at 1 mg/L Ag. The size of the Ag NPs used in this study was 14 ± 6 nm. These particles would be too large to diffuse into the cell, as only the smaller particles mainly in the range of 1–10 nm could enter the cell based on indirect microscopic evidences (Morones et al., 2005). Although electrophoresis studies indicated no direct effect of Ag NPs on intracellular DNA or protein expression (Gogoi et al., 2006), our recent results demonstrated that inhibition by the Ag NPs might be attributed to the accumulation of intracellular ROS (Choi and Hu, 2008).

Bulk silver toxicity is generally governed by the total concentration of labile dissolved intracellular Ag species (Lee et al., 2005). In the cell, silver ions may deactivate cellular enzymes and DNA by reacting with electron-donating groups such as thiol (–SH) groups and generate ROS (Matsumura et al., 2003; Sambhy et al., 2006). Because of its cationic nature and its strong association with various ligands in natural waters, the toxicity of Ag^+ ions depends largely on the strength and amount of the ligands present (Ratte, 1999). The freshly prepared AgCl colloids can be viewed as one of the labile species with respect to their small size and low stability constant ($\log K_1 = 3.3$) in solution (Stumm and Morgan, 1996). Depending on their size and bioavailability, the inhibition caused by AgCl colloids can be as significant as that of Ag^+ ions.

3.7. *Ag NP dissolution*

The time-dependent increases of Ag^+ concentrations and associated color changes of the Ag NP suspension demonstrated the complexity of various processes such as oxidation, crystallization, dissolution and aggregation involved in microbial–nanoparticle interactions. Previous research showed that Ag NPs were susceptible to oxidation by oxygen, and the partially oxidized particles appeared more toxic than the freshly prepared nanoparticles (Lok et al., 2007). Others found, however, that the concentration of Ag^+ decreased by 80% after 24 h, possibly due to Ag^0 cluster formation (Morones et al., 2005). When the Ag NPs were added into a liquid medium, the antimicrobial effectiveness appeared to decrease when compared to that on the agar plates, presumably because of microbial-induced coagulation of nanoparticles (Sondi and Salopek-Sondi, 2004). Experiments involving synthetic zinc sulfide nanoparticles and representative amino acids also indicated a driving role of microbially derived extracellular proteins in rapid nanoparticle aggregation (Moreau et al., 2007). Further research is required to investigate nanoparticle properties such as size, shape, dissolution/aggregation,

Please cite this article as: Choi, O., et al., The inhibitory effects of silver nanoparticles, silver ions, and silver chloride colloids on microbial growth. Water Res. (2008), doi:10.1016/j.watres.2008.02.021

surface coating, and solubility that may affect the specific physicochemical and transport properties, which could exert a significantly different impact on microbial growth (Nel et al., 2006).

3.8. *Environmental application and implication*

The numerous engineered nanomaterials with different sizes, shapes, compositions, and coatings require high-throughput benchmarked protocols to screen for potential hazards in the environment (Maynard et al., 2006). The developed extant respirometric assay and the automatic microtiter assay employed in this research are suitable for toxicity assessment of nanomanterials to microorganisms. The bacteria selected for each assay, however, are generally not exchangeable between the two assays. Because of the intrinsic slow growth rate (about an order of magnitude lower than that of heterotrophs) of autotrophic nitrifying bacteria and their high oxygen uptake (4.3 mg O_2/mg of NH_4^+-N oxidized to nitriate) (Grady et al., 1999), the enriched nitrifying cultures are particularly useful in respirometric assays, but failed to show significant growth in the cell-enumeration-based microtiter assay in this study. In contrast, *E. coli* cells were easily determined with the automatic microtiter assay because of their fast growth rate, but failed to produce meaningful oxygen profiles from the extant respiorometric assay because of the low biomass concentrations from overnight batch cultivation and their low oxygen uptake constants (~0.5 mg O_2/mg COD removed) (Grady et al., 1999).

The results of nanosilver toxicity to environmentally sensitive nitrifying microorganisms suggest that stringent regulations of Ag NPs entering WWTPs are necessary. Nitrifying microorganisms involved in nitrification are critical to biological nutrient removal in modern wastewater treatment. Research is underway to evaluate the fate and impact of Ag NPs in wastewater treatment systems.

4. Conclusions

The nature of the cell growth and oxygen uptake behavior allowed us to determine nanosilver toxicity by applying two independent microbial growth assays—extant respirometric assay and automatic microtiter assay—for nitrifying organisms and *E. coli* cells, respectively. The following conclusions were drawn from this work:

(1) Silver nanoparticles (Ag NPs) strongly inhibited microbial growth. Based on a short-term batch respirometric assay, at 9.3 μM Ag (i.e., 1 mg/L Ag), the inhibitions on nitrifying bacterial growth by Ag NPs, Ag^+ ions, and AgCl colloids were 86±3%, 42±7%, and 46±4%, respectively. Based on a prolonged microtiter assay, at 4.2 μM Ag, the inhibitions on the growth of *E. coli* PHL628-gfp by Ag NPs, Ag^+ ions, and AgCl colloids were 55±8%, 100%, and 66±6%, respectively.
(2) Silver chloride colloids inhibited microbial growth. Depending on their particle size and bioavailability, the inhibition by AgCl colloids can be as significant as that by Ag^+ ions.
(3) There was no evidence of change in cell membrane integrity at 1 mg/L Ag for all of the Ag species tested based on the results from the bacterial LIVE/DEAD assays.

Acknowledgments

This research work was supported by the University of Missouri Research Board and the National Science Foundation under Grant no. 0650943. Any opinions, findings, and conclusions or recommendations expressed in this material are those of the author(s) and do not necessarily reflect the views of the National Science Foundation.

REFERENCES

Adams, L.K., Lyon, D.Y., Alvarez, P.J.J., 2006. Comparative eco-toxicity of nanoscale TiO_2, SiO_2, and ZnO water suspensions. Water Res. 40, 3527–3532.

Blum, D.J.W., Speece, R.E., 1991. A database of chemical toxicity to environmental bacteria and its use in interspecies comparisons and correlations. J. Water Pollut. Control Fed. 63, 198–207.

Chandran, K., Smets, B.F., 2000. Single-step nitrification models erroneously describe batch ammonia oxidation profiles when nitrite oxidation becomes rate limiting. Biotechnol. Bioeng. 68, 396–406.

Choi, O.K., Hu, Z.Q., 2008. Size and ROS dependent nanosilver toxicity to nitrifying bacteria, Environ. Sci. Technol., submitted for publication.

Cole, J.R., Halas, N.J., 2006. Optimized plasmonic nanoparticle distributions for solar spectrum harvesting. Appl. Phys. Lett. 89, 153120.

Creighton, J.A., Eadont, D.G., 1991. Ultraviolet–visible absorption spectra of the colloidal metallic elements. J. Chem. Soc., Faraday Trans. 87, 3881–3891.

Efrima, S., Bronk, B.V., 1998. Silver colloids impregnating or coating bacteria. J. Phys. Chem. B 102, 5947–5950.

Gogoi, S.K., Gopinath, P., Paul, A., Ramesh, A., Ghosh, S.S., Chattopadhyay, A., 2006. Green fluorescent protein-expressing *Escherichia coli* as a model system for investigating the antimicrobial activities of silver nanoparticles. Langmuir 22, 9322–9328.

Grady, C.P.L., Daigger, G.T., Lim, H.C., 1999. Biological Wastewater Treatment, second ed. Marcel Dekker, New York.

Hu, Z.Q., Chandran, K., Grasso, D., Smets, B.F., 2002. Effect of nickel and cadmium speciation on nitrification inhibition. Environ. Sci. Technol. 36, 3074–3078.

Hu, Z.Q., Chandran, K., Grasso, D., Smets, B.F., 2003. Impact of metal sorption and internalization on nitrification inhibition. Environ. Sci. Technol. 37, 728–734.

Hu, Z.Q., Chandran, K., Grasso, D., Smets, B.F., 2004. Comparison of nitrification inhibition by metals in batch and continuous flow reactors. Water Res. 38, 3949–3959.

Junker, L.M., Peters, J.E., Hay, A.G., 2006. Global analysis of candidate genes important for fitness in a competitive biofilm using DNA-array-based transposon mapping. Microbiology—SGM 152, 2233–2245.

Kahraman, M., Yazici, M.M., Sahin, F., Bayrak, O.F., Culha, M., 2007. Reproducible surface-enhanced Raman scattering spectra of bacteria on aggregated silver nanoparticles. Appl. Spectrosc. 61, 479–485.

Kelly, K.L., Coronado, E., Zhao, L.L., Schatz, G.C., 2003. The optical properties of metal nanoparticles: the influence of size, shape, and dielectric environment. J. Phys. Chem. B 107, 668–677.

Please cite this article as: Choi, O., et al., The inhibitory effects of silver nanoparticles, silver ions, and silver chloride colloids on microbial growth. Water Res. (2008), doi:10.1016/j.watres.2008.02.021

Kloepfer, J.A., Mielke, R.E., Nadeau, J.L., 2005. Uptake of CdSe and CdSe/ZnS quantum dots into bacteria via purine-dependent mechanisms. Appl. Environ. Microbiol. 71, 2548–2557.

Kong, H., Jang, J., 2006. One-step fabrication of silver nanoparticle embedded polymer nanofibers by radical-mediated dispersion polymerization. Chem. Commun., 3010–3012.

Lee, D.Y., Fortin, C., Campbell, P.G.C., 2005. Contrasting effects of chloride on the toxicity of silver to two green algae, *Pseudokirchneriella subcapitata* and *Chlamydomonas reinhardtii*. Aquat. Toxicol. 75, 127–135.

Limbach, L.K., Wick, P., Manser, P., Grass, R.N., Bruinink, A., Stark, W.J., 2007. Exposure of engineered nanoparticles to human lung epithelial cells: Influence of chemical composition and catalytic activity on oxidative stress. Environ. Sci. Technol. 41, 4158–4163.

Lok, C.N., Ho, C.M., Chen, R., He, Q.Y., Yu, W.Y., Sun, H.Z., Tam, P.K.H., Chiu, J.F., Che, C.M., 2006. Proteomic analysis of the mode of antibacterial action of silver nanoparticles. J. Proteome Res. 5, 916–924.

Lok, C.N., Ho, C.M., Chen, R., He, Q.Y., Yu, W.Y., Sun, H., Tam, P.K.H., Chiu, J.F., Che, C.M., 2007. Silver nanoparticles: partial oxidation and antibacterial activities. J. Biol. Inorg. Chem. 12, 527–534.

Madigan, M., Martinko, J.M., Parker, J., 2000. Brock Biology of Microorganisms. Prentice Hall, Upper Saddle River, NJ.

Matsumura, Y., Yoshikata, K., Kunisaki, S., Tsuchido, T., 2003. Mode of bactericidal action of silver zeolite and its comparison with that of silver nitrate. Appl. Environ. Microbiol. 69, 4278–4281.

Maynard, A.D., Michelson, E., 2006. The Nanotechnology Consumer Product Inventory 〈http://www.nanotechproject.org/44〉.

Maynard, A.D., Aitken, R.J., Butz, T., Colvin, V., Donaldson, K., Oberdorster, G., Philbert, M.A., Ryan, J., Seaton, A., Stone, V., Tinkle, S.S., Tran, L., Walker, N.J., Warheit, D.B., 2006. Safe handling of nanotechnology. Nature 444, 267–269.

Moreau, J.W., Weber, P.K., Martin, M.C., Gilbert, B., Hutcheon, I.D., Banfield, J.F., 2007. Extracellular proteins limit the dispersal of biogenic nanoparticles. Science 316, 1600–1603.

Morones, J.R., Elechiguerra, J.L., Camacho, A., Holt, K., Kouri, J.B., Ramirez, J.T., Yacaman, M.J., 2005. The bactericidal effect of silver nanoparticles. Nanotechnology 16, 2346–2353.

Nel, A., Xia, T., Madler, L., Li, N., 2006. Toxic potential of materials at the nanolevel. Science 311, 622–627.

Pal, S., Tak, Y.K., Song, J.M., 2007. Does the antibacterial activity of silver nanoparticles depend on the shape of the nanoparticle? A study of the gram-negative bacterium *Escherichia coli*. Appl. Environ. Microbiol. 73, 1712–1720.

Petit, C., Lixon, P., Pileni, M.P., 1993. In-situ synthesis of silver nanocluster in AOT reverse micelles. J. Phys. Chem. 97, 12974–12983.

Priester, J.H., Horst, A.M., Van De Werfhorst, L.C., Saleta, J.L., Mertes, L.A.K., Holden, P.A., 2007. Enhanced visualization of microbial biofilms by staining and environmental scanning electron microscopy. J. Microbiol. Meth. 68, 577–587.

Rand, B.P., Peumans, P., Forrest, S.R., 2004. Long-range absorption enhancement in organic tandem thin-film solar cells containing silver nanoclusters. J. Appl. Phys. 96, 7519–7526.

Ratte, H.T., 1999. Bioaccumulation and toxicity of silver compounds: a review. Environ. Toxicol. Chem. 18, 89–108.

Redwood, P.S., Lead, J.R., Harrison, R.M., Jones, I.P., Stoll, S., 2005. Characterization of humic substances by environmental scanning electron microscopy. Environ. Sci. Technol. 39, 1962–1966.

Sabatini, C.A., Pereira, R.V., Gehlen, M.H., 2007. Fluorescence modulation of acridine and coumarin dyes by silver nanoparticles. J. Fluores. 17, 377–382.

Sambhy, V., MacBride, M.M., Peterson, B.R., 2006. Silver bromide nanoparticle/polymer composites: dual action tunable antimicrobial materials. J. Am. Chem. Soc. 128, 9798–9808.

Savage, N., Diallo, M.S., 2005. Nanomaterials and water purification: opportunities and challenges. J. Nanoparticle Res. 7, 331–342.

Shafer, M.M., Overdier, J.T., Armstong, D.E., 1998. Removal, partitioning, and fate of silver and other metals in wastewater treatment plants and effluent-receiving streams. Environ. Toxicol. Chem. 17, 630–641.

Sondi, I., Salopek-Sondi, B., 2004. Silver nanoparticles as antimicrobial agent: a case study on *E-coli* as a model for Gram-negative bacteria. J. Colloid Interface Sci. 275, 177–182.

Stumm, W., Morgan, J.J., 1996. Aquatic Chemistry: Chemical Equilibria and Rates in Natural Waters, third ed. Wiley, New York.

Wang, J.M., 2003. Interactions of silver with wastewater constituents. Water Res. 37, 4444–4452.

Wenseleers, W., Stellacci, F., Meyer-Friedrichsen, T., Mangel, T., Bauer, C.A., Pond, S.J.K., Marder, S.R., Perry, J.W., 2002. Five orders-of-magnitude enhancement of two-photon absorption for dyes on silver nanoparticle fractal clusters. J. Phys. Chem. B 106, 6853–6863.

Yamaguchi, H., Matsuda, K., Irie, M., 2007. Excited-state behavior of a fluorescent and photochromic diarylethene on silver nonoparticles. J. Phys. Chem. C 111, 3853–3862.

Yamamoto, S., Watarai, H., 2006. Surface-enhanced Raman spectroscopy of dodecanethiol-bound silver nanoparticles at the liquid/liquid interface. Langmuir 22, 6562–6569.

Zhai, H.J., Sun, D.W., Wang, H.S., 2006. Catalytic properties of silica/silver nanocomposites. J. Nanosci. Nanotechnol. 6, 1968–1972.

Please cite this article as: Choi, O., et al., The inhibitory effects of silver nanoparticles, silver ions, and silver chloride colloids on microbial growth. Water Res. (2008), doi:10.1016/j.watres.2008.02.021